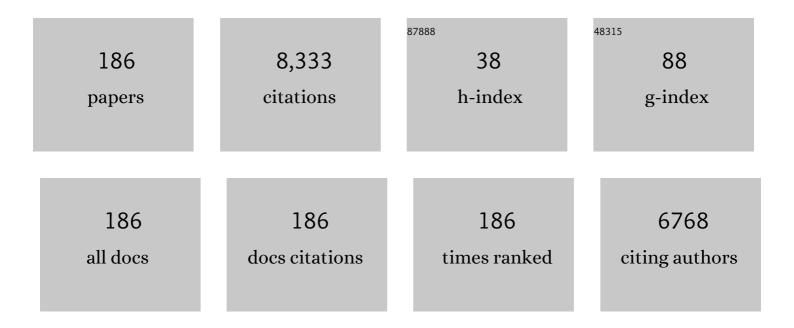
List of Publications by Year in descending order

Source: https://exaly.com/author-pdf/14756/publications.pdf Version: 2024-02-01



CHANCHAN YAN

#	Article	IF	CITATIONS
1	Satellite-derived land surface temperature: Current status and perspectives. Remote Sensing of Environment, 2013, 131, 14-37.	11.0	1,545
2	An Easy-to-Use Airborne LiDAR Data Filtering Method Based on Cloth Simulation. Remote Sensing, 2016, 8, 501.	4.0	723
3	A Review of Current Methodologies for Regional Evapotranspiration Estimation from Remotely Sensed Data. Sensors, 2009, 9, 3801-3853.	3.8	626
4	Analysis of NDVI and scaled difference vegetation index retrievals of vegetation fraction. Remote Sensing of Environment, 2006, 101, 366-378.	11.0	449
5	Land surface emissivity retrieval from satellite data. International Journal of Remote Sensing, 2013, 34, 3084-3127.	2.9	406
6	Watershed Allied Telemetry Experimental Research. Journal of Geophysical Research, 2009, 114, .	3.3	295
7	Review of indirect optical measurements of leaf area index: Recent advances, challenges, and perspectives. Agricultural and Forest Meteorology, 2019, 265, 390-411.	4.8	277
8	Evaluation of MODIS LAI/FPAR Product Collection 6. Part 2: Validation and Intercomparison. Remote Sensing, 2016, 8, 460.	4.0	194
9	Evaluating the fraction of vegetation cover based on NDVI spatial scale correction model. International Journal of Remote Sensing, 2006, 27, 5359-5372.	2.9	153
10	Evaluation of MODIS LAI/FPAR Product Collection 6. Part 1: Consistency and Improvements. Remote Sensing, 2016, 8, 359.	4.0	153
11	Impact of sensor footprint on measurement of directional brightness temperature of row crop canopies. Remote Sensing of Environment, 2013, 134, 135-151.	11.0	145
12	Automatic Extraction of Power Lines From Aerial Images. IEEE Geoscience and Remote Sensing Letters, 2007, 4, 387-391.	3.1	140
13	Soil moisture experiment in the Luan River supporting new satellite mission opportunities. Remote Sensing of Environment, 2020, 240, 111680.	11.0	120
14	Indirect measurement of leaf area index on the basis of path length distribution. Remote Sensing of Environment, 2014, 155, 239-247.	11.0	119
15	Woody-to-total area ratio determination with a multispectral canopy imager. Tree Physiology, 2009, 29, 1069-1080.	3.1	102
16	A novel method for extracting green fractional vegetation cover from digital images. Journal of Vegetation Science, 2012, 23, 406-418.	2.2	99
17	LESS: LargE-Scale remote sensing data and image simulation framework over heterogeneous 3D scenes. Remote Sensing of Environment, 2019, 221, 695-706.	11.0	99
18	Estimating fractional vegetation cover and the vegetation index of bare soil and highly dense vegetation with a physically based method. International Journal of Applied Earth Observation and Geoinformation, 2017, 58, 168-176.	2.8	89

#	Article	IF	CITATIONS
19	Atmospheric water vapor retrieval from Landsat 8 thermal infrared images. Journal of Geophysical Research D: Atmospheres, 2015, 120, 1723-1738.	3.3	85
20	Consistent retrieval methods to estimate land surface shortwave and longwave radiative flux components under clear-sky conditions. Remote Sensing of Environment, 2012, 124, 61-71.	11.0	79
21	A Novel Approach for the Detection of Standing Tree Stems from Plot-Level Terrestrial Laser Scanning Data. Remote Sensing, 2019, 11, 211.	4.0	78
22	Generating Global Products of LAI and FPAR From SNPP-VIIRS Data: Theoretical Background and Implementation. IEEE Transactions on Geoscience and Remote Sensing, 2018, 56, 2119-2137.	6.3	71
23	Design of supercontinuum laser hyperspectral light detection and ranging (LiDAR) (SCLaHS LiDAR). International Journal of Remote Sensing, 2021, 42, 3731-3755.	2.9	71
24	Fractional vegetation cover estimation by using multi-angle vegetation index. Remote Sensing of Environment, 2018, 216, 44-56.	11.0	68
25	Extracting the Green Fractional Vegetation Cover from Digital Images Using a Shadow-Resistant Algorithm (SHAR-LABFVC). Remote Sensing, 2015, 7, 10425-10443.	4.0	66
26	Estimation of surface shortwave radiation components under all sky conditions: Modeling and sensitivity analysis. Remote Sensing of Environment, 2012, 123, 457-469.	11.0	65
27	Angular effect of MODIS emissivity products and its application to the split-window algorithm. ISPRS Journal of Photogrammetry and Remote Sensing, 2011, 66, 498-507.	11.1	63
28	The delineation of agricultural management zones with high resolution remotely sensed data. Precision Agriculture, 2009, 10, 471-487.	6.0	62
29	Improving the estimation of fractional vegetation cover from UAV RGB imagery by colour unmixing. ISPRS Journal of Photogrammetry and Remote Sensing, 2019, 158, 23-34.	11.1	61
30	Topographic radiation modeling and spatial scaling of clear-sky land surface longwave radiation over rugged terrain. Remote Sensing of Environment, 2016, 172, 15-27.	11.0	55
31	Validating GEOV1 Fractional Vegetation Cover Derived From Coarse-Resolution Remote Sensing Images Over Croplands. IEEE Journal of Selected Topics in Applied Earth Observations and Remote Sensing, 2015, 8, 439-446.	4.9	53
32	Filtering Airborne LiDAR Data Through Complementary Cloth Simulation and Progressive TIN Densification Filters. Remote Sensing, 2019, 11, 1037.	4.0	49
33	SLAM-aided forest plot mapping combining terrestrial and mobile laser scanning. ISPRS Journal of Photogrammetry and Remote Sensing, 2020, 163, 214-230.	11.1	45
34	Angular Normalization of Land Surface Temperature and Emissivity Using Multiangular Middle and Thermal Infrared Data. IEEE Transactions on Geoscience and Remote Sensing, 2014, 52, 4913-4931.	6.3	43
35	Regularized inversion method for retrieval of aerosol particle size distribution function in W^1,2 space. Applied Optics, 2006, 45, 7456.	2.1	41
36	Evaluation of Sampling Methods for Validation of Remotely Sensed Fractional Vegetation Cover. Remote Sensing, 2015, 7, 16164-16182.	4.0	40

#	Article	IF	CITATIONS
37	Quantitative Assessment of the Impact of Physical and Anthropogenic Factors on Vegetation Spatial-Temporal Variation in Northern Tibet. Remote Sensing, 2019, 11, 1183.	4.0	40
38	A half-Gaussian fitting method for estimating fractional vegetation cover of corn crops using unmanned aerial vehicle images. Agricultural and Forest Meteorology, 2018, 262, 379-390.	4.8	39
39	Toward operational shortwave radiation modeling and retrieval over rugged terrain. Remote Sensing of Environment, 2018, 205, 419-433.	11.0	38
40	Spatial distribution of net primary productivity and evapotranspiration in Changbaishan Natural Reserve, China, using Landsat ETM+ data. Canadian Journal of Remote Sensing, 2004, 30, 731-742.	2.4	35
41	Temporal Extrapolation of Daily Downward Shortwave Radiation Over Cloud-Free Rugged Terrains. Part 1: Analysis of Topographic Effects. IEEE Transactions on Geoscience and Remote Sensing, 2018, 56, 6375-6394.	6.3	34
42	Efficient registration of terrestrial LiDAR scans using a coarse-to-fine strategy for forestry applications. Agricultural and Forest Meteorology, 2016, 225, 8-23.	4.8	33
43	Separating vegetation and soil temperature using airborne multiangular remote sensing image data. International Journal of Applied Earth Observation and Geoinformation, 2012, 17, 66-75.	2.8	32
44	A Large-Scale Emulation System for Realistic Three-Dimensional (3-D) Forest Simulation. IEEE Journal of Selected Topics in Applied Earth Observations and Remote Sensing, 2017, 10, 4834-4843.	4.9	32
45	Modeling surface longwave radiation over high-relief terrain. Remote Sensing of Environment, 2020, 237, 111556.	11.0	32
46	Estimation of surface upward longwave radiation from MODIS and VIIRS clear-sky data in the Tibetan Plateau. Remote Sensing of Environment, 2015, 162, 221-237.	11.0	31
47	Quantifying Understory and Overstory Vegetation Cover Using UAV-Based RGB Imagery in Forest Plantation. Remote Sensing, 2020, 12, 298.	4.0	31
48	Empirical Algorithms to Map Global Broadband Emissivities Over Vegetated Surfaces. IEEE Transactions on Geoscience and Remote Sensing, 2013, 51, 2619-2631.	6.3	29
49	Performance evaluation of four directional emissivity analytical models with thermal SAIL model and airborne images. Optics Express, 2015, 23, A346.	3.4	29
50	Using Airborne Laser Scanner and Path Length Distribution Model to Quantify Clumping Effect and Estimate Leaf Area Index. IEEE Transactions on Geoscience and Remote Sensing, 2018, 56, 3196-3209.	6.3	29
51	Performance stability of the MODIS and VIIRS LAI algorithms inferred from analysis of long time series of products. Remote Sensing of Environment, 2021, 260, 112438.	11.0	29
52	Seed point set-based building roof extraction from airborne LiDAR point clouds using a top-down strategy. Automation in Construction, 2021, 126, 103660.	9.8	28
53	A bi-directional gap model for simulating the directional thermal radiance of row crops. Science in China Series D: Earth Sciences, 2002, 45, 1087-1098.	0.9	27
54	Estimation of forest leaf area index using terrestrial laser scanning data and path length distribution model in open-canopy forests. Agricultural and Forest Meteorology, 2018, 263, 323-333.	4.8	26

#	Article	IF	CITATIONS
55	Image-based 3D corn reconstruction for retrieval of geometrical structural parameters. International Journal of Remote Sensing, 2009, 30, 5505-5513.	2.9	25
56	Estimating the leaf area of an individual tree in urban areas using terrestrial laser scanner and path length distribution model. ISPRS Journal of Photogrammetry and Remote Sensing, 2018, 144, 357-368.	11.1	25
57	Scale Effect in Indirect Measurement of Leaf Area Index. IEEE Transactions on Geoscience and Remote Sensing, 2016, 54, 3475-3484.	6.3	24
58	Estimating structural parameters of agricultural crops from ground-based multi-angular digital images with a fractional model of sun and shade components. Agricultural and Forest Meteorology, 2017, 246, 162-177.	4.8	24
59	Retrieval of Global Orbit Drift Corrected Land Surface Temperature from Long-term AVHRR Data. Remote Sensing, 2019, 11, 2843.	4.0	24
60	Characterizing reflectance anisotropy of background soil in open-canopy plantations using UAV-based multiangular images. ISPRS Journal of Photogrammetry and Remote Sensing, 2021, 177, 263-278.	11.1	23
61	Cloth simulation-based construction of pit-free canopy height models from airborne LiDAR data. Forest Ecosystems, 2020, 7, .	3.1	23
62	Evaluation of the Vegetation-Index-Based Dimidiate Pixel Model for Fractional Vegetation Cover Estimation. IEEE Transactions on Geoscience and Remote Sensing, 2022, 60, 1-14.	6.3	22
63	Sensitivity of Topographic Correction to the DEM Spatial Scale. IEEE Geoscience and Remote Sensing Letters, 2015, 12, 53-57.	3.1	20
64	A simple terrain relief index for tuning slope-related parameters of LiDAR ground filtering algorithms. ISPRS Journal of Photogrammetry and Remote Sensing, 2018, 143, 181-190.	11.1	20
65	Improved Methods for Spectral Calibration of On-Orbit Imaging Spectrometers. IEEE Transactions on Geoscience and Remote Sensing, 2010, , .	6.3	19
66	The Complicate Observations and Multi-Parameter Land Information Constructions on Allied Telemetry Experiment (COMPLICATE). PLoS ONE, 2015, 10, e0137545.	2.5	19
67	Thermal bidirectional gap probability model for row crop canopies and validation. Science in China Series D: Earth Sciences, 2003, 46, 1241-1249.	0.9	18
68	Implications of Whole-Disc DSCOVR EPIC Spectral Observations for Estimating Earth's Spectral Reflectivity Based on Low-Earth-Orbiting and Geostationary Observations. Remote Sensing, 2018, 10, 1594.	4.0	16
69	Extracting Leaf Area Index by Sunlit Foliage Component from Downward-Looking Digital Photography under Clear-Sky Conditions. Remote Sensing, 2015, 7, 13410-13435.	4.0	15
70	Improved Topographic Normalization for Landsat TM Images by Introducing the MODIS Surface BRDF. Remote Sensing, 2015, 7, 6558-6575.	4.0	15
71	Determination of Optimum Viewing Angles for the Angular Normalization of Land Surface Temperature over Vegetated Surface. Sensors, 2015, 15, 7537-7570.	3.8	15
72	Scaling of FAPAR from the Field to the Satellite. Remote Sensing, 2016, 8, 310.	4.0	15

#	Article	IF	CITATIONS
73	Estimating Leaf Angle Distribution From Smartphone Photographs. IEEE Geoscience and Remote Sensing Letters, 2019, 16, 1190-1194.	3.1	15
74	An Operational Method for Validating the Downward Shortwave Radiation Over Rugged Terrains. IEEE Transactions on Geoscience and Remote Sensing, 2020, , 1-18.	6.3	15
75	Modeling the radiation regime of a discontinuous canopy based on the stochastic radiative transport theory: Modification, evaluation and validation. Remote Sensing of Environment, 2021, 267, 112728.	11.0	15
76	Reconstruction of Single Tree with Leaves Based on Terrestrial LiDAR Point Cloud Data. Remote Sensing, 2018, 10, 686.	4.0	14
77	Single Scanner BLS System for Forest Plot Mapping. IEEE Transactions on Geoscience and Remote Sensing, 2021, 59, 1675-1685.	6.3	14
78	A Bibliometric Visualization Review of the MODIS LAI/FPAR Products from 1995 to 2020. Journal of Remote Sensing, 2021, 2021, .	6.7	14
79	Quantitative Evaluation of Leaf Inclination Angle Distribution on Leaf Area Index Retrieval of Coniferous Canopies. Journal of Remote Sensing, 2021, 2021, .	6.7	14
80	A novel and efficient method for wood–leaf separation from terrestrial laser scanning point clouds at the forest plot level. Methods in Ecology and Evolution, 2021, 12, 2473-2486.	5.2	14
81	Modeling directional effects from nonisothermal land surfaces in wideband thermal infrared measurements. IEEE Transactions on Geoscience and Remote Sensing, 2001, 39, 1095-1099.	6.3	13
82	Estimation of Canopy and Woody Components Clumping Indices at Three Mature <i>Picea crassifolia</i> Forest Stands. IEEE Journal of Selected Topics in Applied Earth Observations and Remote Sensing, 2015, 8, 1413-1422.	4.9	13
83	An Iterative-Mode Scan Design of Terrestrial Laser Scanning in Forests for Minimizing Occlusion Effects. IEEE Transactions on Geoscience and Remote Sensing, 2021, 59, 3547-3566.	6.3	13
84	Quantification of occlusions influencing the tree stem curve retrieving from single-scan terrestrial laser scanning data. Forest Ecosystems, 2019, 6, .	3.1	13
85	Thermal bidirectional gap probability model for row crop canopies and validation. Science in China Series D: Earth Sciences, 2003, 46, 1241.	0.9	13
86	A portable Multi-Angle Observation System. , 2012, , .		12
87	Noise Evaluation of early images for Landsat 8 Operational Land Imager. Optics Express, 2014, 22, 27270.	3.4	12
88	Potentials and Limits of Vegetation Indices With BRDF Signatures for Soil-Noise Resistance and Estimation of Leaf Area Index. IEEE Transactions on Geoscience and Remote Sensing, 2020, 58, 5092-5108.	6.3	12
89	Improving the estimation of canopy cover from UAV-LiDAR data using a pit-free CHM-based method. International Journal of Digital Earth, 2021, 14, 1477-1492.	3.9	12
90	Evaluation of Radiometric Performance for the Thermal Infrared Sensor Onboard Landsat 8. Remote Sensing, 2014, 6, 12776-12788.	4.0	11

#	Article	IF	CITATIONS
91	Modeling of Land Surface Thermal Anisotropy Based on Directional and Equivalent Brightness Temperatures Over Complex Terrain. IEEE Journal of Selected Topics in Applied Earth Observations and Remote Sensing, 2019, 12, 410-423.	4.9	11
92	A Scaling-Based Method for the Rapid Retrieval of FPAR From Fine-Resolution Satellite Data in the Remote-Sensing Trend-Surface Framework. IEEE Transactions on Geoscience and Remote Sensing, 2020, 58, 7035-7048.	6.3	11
93	Quantitative Analysis of Terrain Reflected Solar Radiation in Snow overed Mountains: A Case Study in Southeastern Tibetan Plateau. Journal of Geophysical Research D: Atmospheres, 2021, 126, e2020JD034294.	3.3	11
94	Research on scale effect of histogram. Science in China Series D: Earth Sciences, 2002, 45, 949.	0.9	10
95	A Contextual Fire Detection Algorithm for Simulated HJ-1B Imagery. Sensors, 2009, 9, 961-979.	3.8	10
96	A three-channel algorithm for retrieving night-time land surface temperature from MODIS data under thin cirrus clouds. International Journal of Remote Sensing, 2015, 36, 4836-4863.	2.9	10
97	Global Land Surface Evapotranspiration Estimation From Meteorological and Satellite Data Using the Support Vector Machine and Semiempirical Algorithm. IEEE Journal of Selected Topics in Applied Earth Observations and Remote Sensing, 2018, 11, 513-521.	4.9	10
98	Estimation of Daily Average Downward Shortwave Radiation over Antarctica. Remote Sensing, 2018, 10, 422.	4.0	10
99	Extension of the Generalized Split-Window Algorithm for Land Surface Temperature Retrieval to Atmospheres With Heavy Dust Aerosol Loading. IEEE Journal of Selected Topics in Applied Earth Observations and Remote Sensing, 2015, 8, 825-834.	4.9	9
100	Daytime Land Surface Temperature Extraction from MODIS Thermal Infrared Data under Cirrus Clouds. Sensors, 2015, 15, 9942-9961.	3.8	9
101	Quantitative Analysis of Aerosol Influence on Suomi-NPP VIIRS Nighttime Light in China. IEEE Journal of Selected Topics in Applied Earth Observations and Remote Sensing, 2020, 13, 3557-3568.	4.9	9
102	Assessing the Accuracy of Landsat-MODIS NDVI Fusion with Limited Input Data: A Strategy for Base Data Selection. Remote Sensing, 2021, 13, 266.	4.0	9
103	High Spatial Resolution and High Temporal Frequency (30-m/15-day) Fractional Vegetation Cover Estimation over China Using Multiple Remote Sensing Datasets: Method Development and Validation. Journal of Meteorological Research, 2021, 35, 128-147.	2.4	9
104	Global quasi-daily fractional vegetation cover estimated from the DSCOVR EPIC directional hotspot dataset. Remote Sensing of Environment, 2022, 269, 112835.	11.0	9
105	Ultrahigh-resolution boreal forest canopy mapping: Combining UAV imagery and photogrammetric point clouds in a deep-learning-based approach. International Journal of Applied Earth Observation and Geoinformation, 2022, 107, 102686.	2.8	9
106	Application of ensemble kalman filter to geophysical parameters retrieval in remote sensing: A case study of kernel-driven BRDF model inversion. Science in China Series D: Earth Sciences, 2006, 49, 632-640.	0.9	8
107	A Practical Two-Stage Algorithm for Retrieving Land Surface Temperature from AMSR-E Data—A Case Study Over China. IEEE Journal of Selected Topics in Applied Earth Observations and Remote Sensing, 2018, 11, 1939-1948.	4.9	8
108	Spatial Scale Consideration for Estimating All-Sky Surface Shortwave Radiation With a Modified 1-D Radiative Transfer Model. IEEE Journal of Selected Topics in Applied Earth Observations and Remote Sensing, 2019, 12, 821-835.	4.9	7

#	Article	IF	CITATIONS
109	A remote sensing method for retrieving land surface emissivity and temperature in cloudy areas: a case study over South China. International Journal of Remote Sensing, 2019, 40, 1724-1735.	2.9	7
110	Clumping Effects in Leaf Area Index Retrieval From Large-Footprint Full-Waveform LiDAR. IEEE Transactions on Geoscience and Remote Sensing, 2022, 60, 1-20.	6.3	7
111	Indirect Measurement of Forest Leaf Area Index Using Path Length Distribution Model and Multispectral Canopy Imager. IEEE Journal of Selected Topics in Applied Earth Observations and Remote Sensing, 2016, 9, 2532-2539.	4.9	6
112	Integration of two semi-physical models of terrestrial evapotranspiration using the China Meteorological Forcing Dataset. International Journal of Remote Sensing, 2019, 40, 1966-1980.	2.9	6
113	Foreword to the Special Issue on The Recent Progress in Quantitative Land Remote Sensing: Modeling and Estimation. IEEE Journal of Selected Topics in Applied Earth Observations and Remote Sensing, 2019, , 1-5.	4.9	6
114	A strategy to integrate <i>a priori</i> knowledge for an improved inversion of the LAI from BRDF modelling. International Journal of Remote Sensing, 2008, 29, 4927-4941.	2.9	5
115	Analysis on the inversion accuracy of LAI based on simulated point clouds of terrestrial LiDAR of tree by ray tracing algorithm. , 2013, , .		5
116	From Geometric-Optical Remote Sensing Modeling to Quantitative Remote Sensing Science—In Memory of Academician Xiaowen Li. Remote Sensing, 2018, 10, 1764.	4.0	5
117	A Machine Learning Approach to Crater Classification from Topographic Data. Remote Sensing, 2019, 11, 2594.	4.0	5
118	Extending a Linear Kernel-Driven BRDF Model to Realistically Simulate Reflectance Anisotropy Over Rugged Terrain. IEEE Transactions on Geoscience and Remote Sensing, 2022, 60, 1-16.	6.3	5
119	Influencing Factors in Estimation of Leaf Angle Distribution of an Individual Tree from Terrestrial Laser Scanning Data. Remote Sensing, 2021, 13, 1159.	4.0	5
120	<title>Digital simulation for low-light-level night vision imaging system</title> . , 2000, , .		4
121	An airborne multi-angle power line inspection system. , 2007, , .		4
122	A modified vegetation index based algorithm for thermal imagery sharpening. , 2010, , .		4
123	A novel building boundary reconstruction method based on lidar data and images. , 2013, , .		4
124	Recent Progress in Quantitative Land Remote Sensing in China. Remote Sensing, 2018, 10, 1490.	4.0	4
125	Modified gap fraction model of individual trees for estimating leaf area using terrestrial laser scanner. Journal of Applied Remote Sensing, 2017, 11, 1.	1.3	4
126	Correcting Crown-Level Clumping Effect for Improving Leaf Area Index Retrieval From Large-Footprint LiDAR: A Study Based on the Simulated Waveform and GLAS Data. IEEE Journal of Selected Topics in Applied Earth Observations and Remote Sensing, 2021, 14, 12386-12402.	4.9	4

#	Article	IF	CITATIONS
127	Using a Vegetation Index-Based Mixture Model to Estimate Fractional Vegetation Cover Products by Jointly Using Multiple Satellite Data: Method and Feasibility Analysis. Forests, 2022, 13, 691.	2.1	4
128	Classification-based fusion of IKONOS 1-m high-resolution panchromatic image and 4-m multi-spectral images. , 0, , .		3
129	Validation of MODIS albedo product by using field measurements and airborne multi-angular remote sensing observations. , 0, , .		3
130	Uncertainty and sensitivity ratio of parameters in estimating and promoting retrieval accuracy. International Journal of Remote Sensing, 2008, 29, 4891-4905.	2.9	3
131	A method for leaf gap fraction estimation based on multispectral digital images from Multispectral Canopy Imager. , 2011, , .		3
132	A comparison of different optimization algorithms for retrieving aerosol optical depths from satellite data: an example of using a dual-angle algorithm. International Journal of Remote Sensing, 2011, 32, 8949-8968.	2.9	3
133	Accuracy evaluation of the ground-based fractional vegetation cover measurement by using simulated images. , 2012, , .		3
134	Spectral Recalibration for In-Flight Broadband Sensor Using Man-Made Ground Targets. IEEE Transactions on Geoscience and Remote Sensing, 2013, 51, 4316-4329.	6.3	3
135	Recovering land surface temperature under cloudy skies for potentially deriving surface emitted longwave radiation by fusing MODIS and AMSR-E measurements. , 2014, , .		3
136	Shortwave radiative transfer modeling at large scale for partial cloudy conditions. , 2015, , .		3
137	Toward a general method for detecting clouds and shadows in optical remote sensing imagery. , 2016, , \cdot		3
138	Spatial scale effect on vegetation phenological analysis using remote sensing data. , 2016, , .		3
139	Retrieving K-Band Instantaneous Microwave Land Surface Emissivity Based on Passive Microwave Brightness Temperature and Atmospheric Precipitable Water Vapor Data. IEEE Journal of Selected Topics in Applied Earth Observations and Remote Sensing, 2017, 10, 5608-5617.	4.9	3
140	Global land surface evapotranspiration estimation from MERRA dataset and MODIS product using the support vector machine. , 2017, , .		3
141	Generating Long Time Series of High Spatiotemporal Resolution FPAR Images in the Remote Sensing Trend Surface Framework. IEEE Transactions on Geoscience and Remote Sensing, 2022, 60, 1-15.	6.3	3
142	Human Activity Changes During COVIDâ€19 Lockdown in China—A View From Nighttime Light. GeoHealth, 2022, 6, .	4.0	3
143	Fractional vegetation cover retrieval using multi-spatial resolution data and plant growth model. , 2010, , .		2
144	Clear sky Net Surface Radiative Fluxes over rugged terrain from satellite measurements. , 2011, , .		2

9

#	Article	IF	CITATIONS
145	Generation of pixel-level resolution lunar DEM based on Chang'E-1 three-line imagery and laser altimeter data. Computers and Geosciences, 2013, 59, 53-59.	4.2	2
146	Estimation of fractional vegetation cover using mean-based spectral unmixing method. , 2017, , .		2
147	Information content of multi-angular remote sensing data. , 0, , .		1
148	Uncertainty of remote sensing model inversion and a synthetical inverse scenario. , 0, , .		1
149	Retrieval of aerosol optical depth and single scattering albedo from AMTIS imagery. , 0, , .		1
150	Retrieval of LAI by assimilating remotely sensed data into a simple crop growth model. , 2007, , .		1
151	Automatic block generation and 3D line extraction in photogrammetric power line inspection. , 2007, , \cdot		1
152	Retrieval of time series LAI by coupling an empirical crop growth model with a radiative transfer model. , 2010, , .		1
153	Extending RGM to simulate the directional reflectance for complex mountainous regions. , 2012, , .		1
154	Analyzing the characteristics of FPAR from maize canopies measured in Northwest China. , 2013, , .		1
155	Error analysis for emissivity measurement using FTIR spectrometer. , 2013, , .		1
156	Realistic 3D-simulation of large-scale forest scene based on individual tree detection. , 2016, , .		1
157	Clobal land surface evapotranspiration estimation from meteorological and satellite data using the support vector machine. , 2016, , .		1
158	Simulating Spectral Images with Less Model Through a Voxel-Based Parameterization of Airborne Lidar Data. , 2019, , .		1
159	Ground-Based Radiation Observational Method in Mountainous Areas. , 2019, , .		1
160	A priori knowledge in the inversion of linear kernel-driven BRDF models. , 0, , .		0
161	Effects of GA on the inversion of linear and nonlinear remote sensing models. , 0, , .		0
162	Leaf area index inversion using multiangular and multispectral data sets. , 0, , .		0

10

#	Article	IF	CITATIONS
163	An iterative temperature inversion method for nonisothermal land surfaces. , 0, , .		0
164	Atmospheric correction for AMTIS single-channel multi-angular thermal-infrared imagery. , 0, , .		0
165	A sensitivity criterion for BRDF model inversion analysis. , 0, , .		Ο
166	Modeling vegetation cover distribution at different scales based on bayesian statistical inference. , 0, ,		0
167	Extraction of tree height from large viewing angle aerial images. , 2005, , .		0
168	Use of airborne hyperspectral imagery to investigate the influence of soil nitrogen supplies and variable-rate fertilization to winter wheat growth. Proceedings of SPIE, 2007, 6742, 216.	0.8	0
169	Automatic 3D power line reconstruction of multi-angular imaging power line inspection system. Proceedings of SPIE, 2007, 6752, 597.	0.8	0
170	Kernel based simplification of canopy reflectance model using partial least square regression. Proceedings of SPIE, 2007, , .	0.8	0
171	Water storage changes over great lake from satellite gravimetry and tidal data. , 2012, , .		Ο
172	Validation of coarse-resolution Fractional Vegetation Cover product in Heihe basin, China. , 2013, , .		0
173	Topographic correction of retrieved surface shortwave radiative fluxes from space under clear-sky conditions. , 2014, , .		Ο
174	Influence of thin cirrus clouds on land surface temperture retrieval using the generalized split-window algorithm from thermal infrared data. , 2014, , .		0
175	Estimation of daytime land surface temperature from space radiometer under thin cirrus cloudy skies. , 2015, , .		0
176	Indirect measurement of forest leaf area index using path length model and Multispectral Canopy Imager. , 2015, , .		0
177	A simple fusion algorithm of polar-orbiting and geostationary satellite data for the estimation of surface shortwave fluxes. , 2016, , .		0
178	An algorithm for retrieving instantaneous microwave land surface emissivity from passive microwave brightness temperature and precipitable water vapor data. , 2016, , .		0
179	Remote Sensing Modelling and Parameter Inversion. Springer Geography, 2017, , 323-338.	0.4	0
180	An algorithm for retrieving land surface temperature from AMSR-E data over the desert regions. , 2017, , .		0

#	Article	IF	CITATIONS
181	Modeling Surface Thermal Anisotropy Using Brightness Temperature over Complex Terrains. , 2018, , .		Ο
182	Estimation of Annual Averaged Evapotranspiration by Using Passive Microwave Observations. , 2018, , .		0
183	Analysis of the Kernel-Driven Brdf Model Over Rugged Terrains. , 2019, , .		Ο
184	Extraction Of Urban And Rural Based On Globaland30. , 2019, , .		0
185	Analysis of the Influence of Leaf Inclination Angle Distribution on the Leaf Area Inversion of Isolated Tree Based on Terrestrial Laser Scanning. , 2021, , .		Ο
186	A Cloud Detection Algorithm for Tiangong-2 Remote Sensing Data Over the Tibetan Plateau. Lecture Notes in Electrical Engineering, 2019, , 82-93.	0.4	0